# Study of superelastic performance on novel (Ti-Zr)-based alloy: Influence of thermal treatment time

J.J. Gao, P. Castany*, D. Laillé, I. Thibon, T. Gloriant

Univ Rennes, INSA Rennes, CNRS, ISCR UMR 6226, 35000 Rennes

* philippe.castany@insa-rennes.fr

## Abstract

In this study, the superelastic performance of a novel metastable β Ti-20Zr-3Mo-3Sn alloy (at.%) displaying stress-induced α" martensitic (SIM) transformation is investigated by resistivity, cyclic tensile tests and electron back-scattered diffraction (EBSD) for three different solution treatment durations: 5 min, 30 min and 60 min at 700°C. EBSD observations reveal that the Ti-20Zr-3Mo-3Sn alloy presents different recrystallization texture in the three conditions while keeping the optimal <110>$_\beta$ direction along the rolling direction. All the samples displayed high recovery strain which is more than 3.0%. However, the shortest heat treatment time allows to stabilize the superelastic behavior at this maximum value for a wide range of applied strain.

## 1. Introduction

NiTi family alloys are commonly used for the manufacture of biomedical devices such as orthodontic arches, orthopedic staples, endovascular stents and so on, owing to their superelastic property. However, nickel hypersensitivity and toxicity still remain a problem in terms of biocompatibility [1] and superelastic β-titanium alloys are now considered as the best alternative material for biomedical applications. Consequently, numerous Ni-free superelastic (Ti-Nb)-based alloys composed of non-cytotoxic alloying elements are widely studied, for example Ti–Nb–Al, Ti–Nb–Zr, Ti–Nb–Ta, Ti-Nb-O, Ti-Nb-N, Ti-Nb-Zr-Sn, Ti–Nb–Zr–Ta, Ti–Nb–Ta–Zr–O [2-10]. Unfortunately, the superelastic property observed is less than that of NiTi alloys and does not exceed 3.0% of recovery strain in (Ti-Nb)-based alloys. In fact, superelasticity is due to the reversible martensitic transformation from the body-centered cubic β phase (austenite) to the C-centered orthorhombic α" martensitic phase [2]. Recently, it was reported that replacing niobium as the main alloying element by hafnium [11] or zirconium [12, 13] could be an effective method to improve the superelastic performance of Ni-free titanium-based alloys. Indeed, the martensitic transformation start temperature ($M_S$) can be controlled through the substitution of niobium by zirconium in order to promote superelasticity at room temperature and the recovery strain as high as 7.0% could be achieved in some optimized chemical compositions [13]. In this work, a quaternary superelastic Ti-20Zr-3Mo-3Sn (at.%) alloy was designed with high zirconium content. Molybdenum is added as b stabilizing element to decrease the $M_S$ temperature in order to obtain superelasticity at room temperature. Tin is added to suppress the ω phase formation [12].

## 2. Material and methods

The Ti-20Zr-3Mo-3Sn alloy (at.%) was synthesized by cold crucible levitation melting (CCLM) technique under argon atmosphere. In this work, 99.95% pure titanium, 99.078% pure zirconium, 99.9% pure molybdenum and 99.99% pure tin were used as raw materials. After melting, ingot was homogenized at 950°C for 1200 min under high vacuum ($10^{-7}$ mbar), followed by water quenching. One-way cold rolling operation was applied until 95% reduction rate in thickness at room temperature. Dog-bone tensile specimens were machined from the cold-rolled sheets with normalized shape of 3.0 mm × 0.5 mm × 15.0 mm. In order to restore a fully recrystallized microstructure from the cold-rolled state, the tensile specimens were finally solution-treated under high vacuum ($10^{-7}$ mbar) for 3 different durations (t=5, 30, and 60 min) at 700°C in the β-phase domain followed by water quenching in order to retain the β phase in its metastable state.

In this investigation, the solution treatment temperature was chosen near but a little higher than the β transus temperature of Ti-20Zr-3Mo-3Sn alloy, which was obtained by measuring the electrical resistivity variation upon temperature. Indeed, electrical resistivity, which is very sensitive to microstructural changes, is an effective thermal analysis technique for detecting such b transus temperature [14]. Fig. 1 shows the typical hysteresis loop obtained between 400°C and 900°C during a heating/cooling cycle. As showed on this resistivity curve, the β transus temperature is measured at 690°C for the studied Ti-20Zr-3Mo-3Sn alloy.

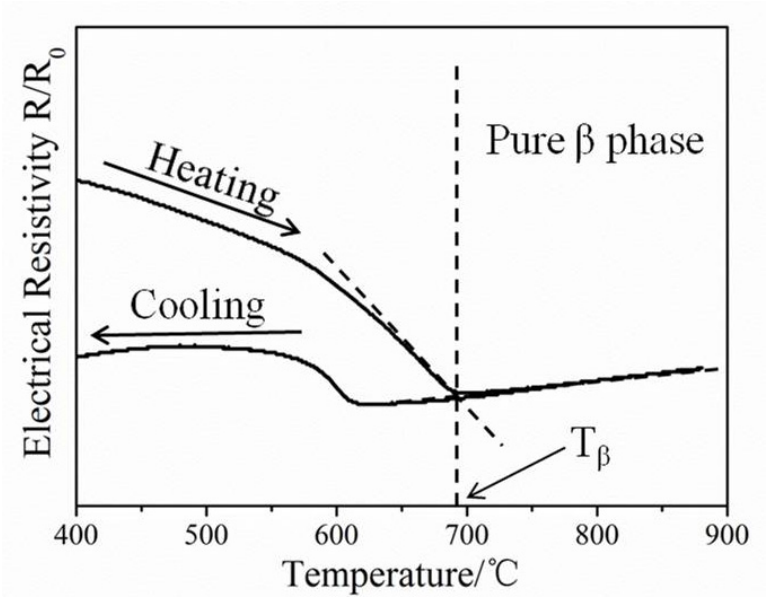


**Fig.1. Electrical resistivity curve of as-rolled Ti-20Zr-3Mo-3Sn alloy during heating and cooling.**

Cyclic loading/unloading tensile tests with a strain rate of $10^{-4}$ $s^{-1}$ were particularly conducted in order to characterize the superelastic behavior of the Ti-20Zr-3Mo-3Sn alloy after the different thermal treatments. Cyclic tensile tests consist of strain increment steps of 0.5% followed by stress releasing up to the elongation of 5.0%. The tensile direction was chosen parallel to the cold rolling direction. An extensometer was used to ensure the accuracy of strain measurements during these tests.

Microstructure after different solution treatments was investigated by electron back-scattered diffraction (EBSD) analyses in a scanning electron microscope (Jeol JSM 7100F, SEM) equipped with an Oxford HKL EBSD system. Prior to the EBSD observations, all the specimens were firstly mechanically mirror-polished by using several SiC papers and then followed by colloidal silica suspension mixed with $H_2O_2$ solution.

## 3. Results

Fig. 2 presents the engineering stress-strain curves obtained from cyclic tensile tests for samples subjected to three different thermal treatments: 700°C for 5 min (ST-700-05, Fig. 2a), 700°C for 30 min (ST-700-30, Fig. 2b) and 700°C for 60 min (ST-700-60, Fig. 2c). All the curves show large recovery strains after unloading. The presence of hysteresis loops in the tensile curves between loading and unloading are due to the reversible SIM transformation between β and SIM α" phase. The Young's modulus and critical stress for introducing martensite transformation are 52GPa, 50GPa, 55GPa and 600MPa, 590MPa, 560MPa for the ST-700-05, ST-700-30 and ST-700-60 conditions, respectively. The Fig. 2(d) reveals recovery strain for each cycle as a function of applied strain. For the first three cycles, i.e. until 1.5% of applied strain, all curves show a perfect superelastic behavior, as the applied strain is fully recovered. When the applied strain exceeds 2.0%, residual strain is detected. The ST-700-60 condition exhibits the lower recoverable strain, reaching 3.0% for 4.5% of applied strain. For the two other conditions, the behavior is very similar until 3.5% of applied strain: Both materials keep a full reversibility of the deformation until 2.5% of applied strain, while a few amount of residual strain appears for higher applied strain. These two conditions allow a maximum recovery strain of 3.2% for 3.5-4% of applied strain. However, the value of recovery strain immediately decreases when increasing the applied strain for the ST-700-30 condition, while the recovery strain keeps its maximum value for the ST-700-05 condition. The ST-700-05 condition is thus the one leading to the maximum and the more stable superelastic behavior.

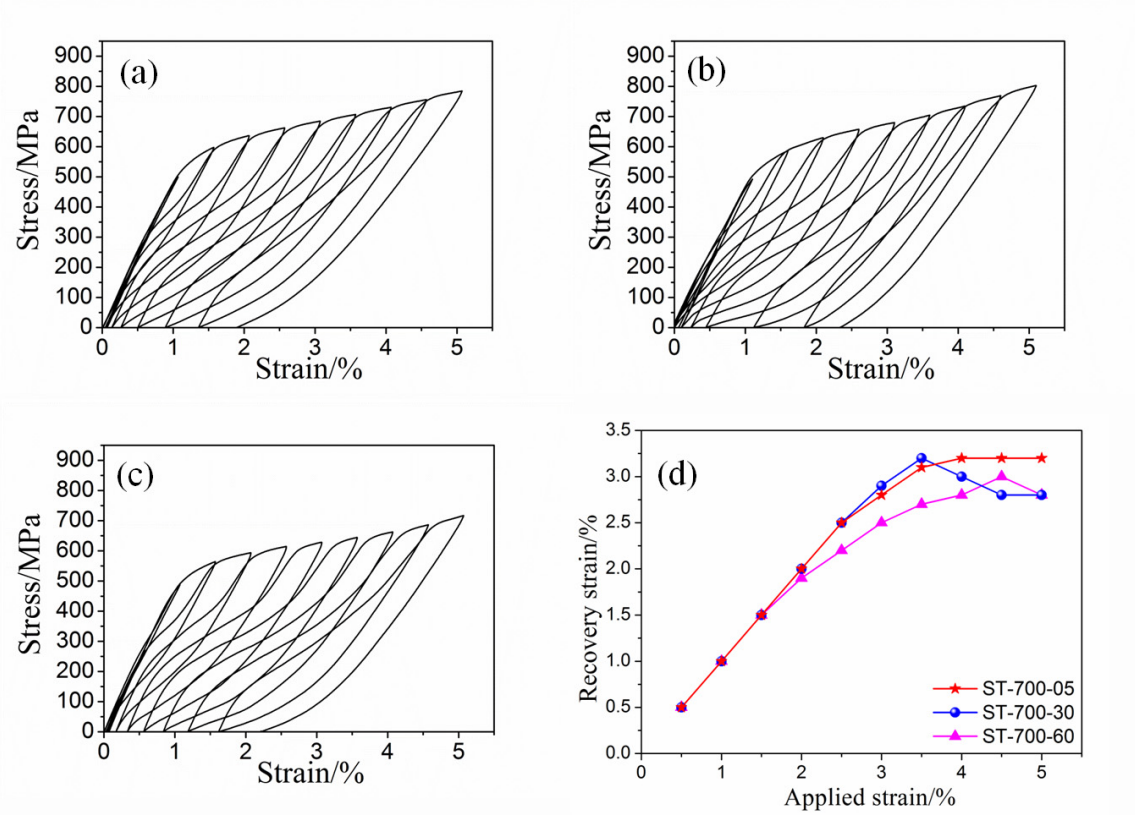


**Fig. 2. Engineering stress-strain curves obtained from cyclic tensile tests at room temperature: (a) ST-700-05; (b) ST-700-30; (c) ST-700-60. (d) Variation of recovery strain as a function of applied strain for different thermo-mechanical conditions.**

Cold rolling, as a severe plastic deformation process, promotes specific crystallographic orientations of most of grains after recrystallization, leading to the formation of texture. The EBSD inverse pole figure (IPF) maps for the rolling direction of the three different thermo-mechanical treatments are shown in Fig. 3(a-c) corresponding to ST-700-05, ST-700-30 and ST-700-60 conditions, respectively. All the samples show a typical equiaxed β-grain microstructure and the predominant green color is observed, indicating a dominant of $\{hkl\}_\beta<110>_\beta$ texture is formed. In order to determine the recrystallized textures precisely, the ODF (orientation distribution function) were calculated for each sample. Corresponding IPF of rolling direction (RD) and normal direction (ND) are shown in Fig. 4 for each thermal treatment in order to highlight each texture. The main texture component is $<110>_\beta\{211\}_\beta$ for the ST-700-05 (Fig. 4a), $<110>_\beta\{111\}_\beta$ for the ST-700-30 (Fig. 4b) and $<110>_\beta\{001\}_\beta$ for the ST-700-60 (Fig. 4c). It is worth noting that the rolling direction keeps the same crystallographic orientation while the normal direction strongly changes depending on heat treatment time.

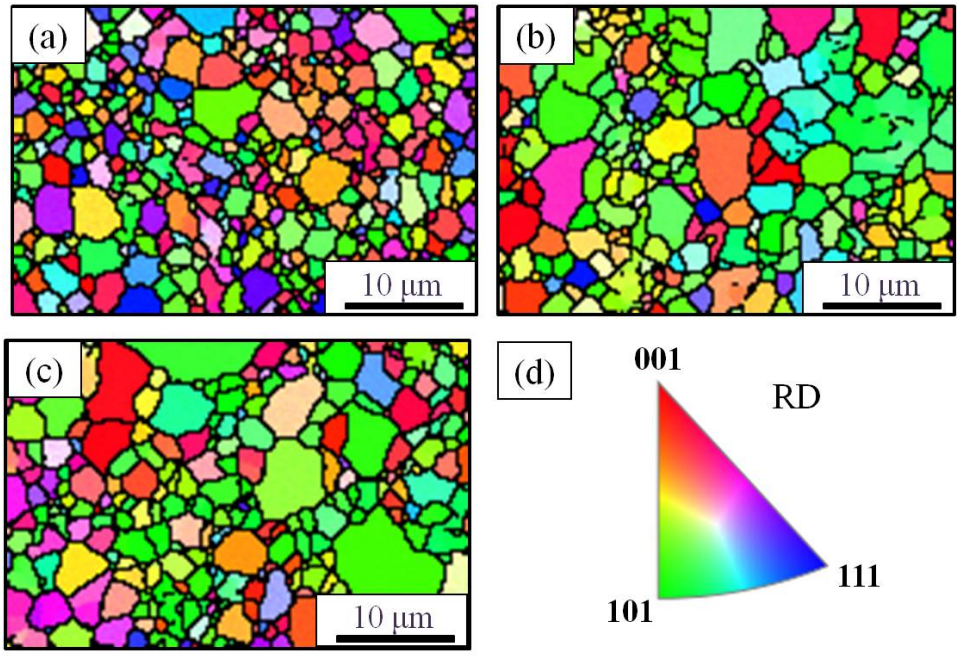


**Fig. 3. EBSD RD (Rolling Direction) IPF maps of solution treated samples: (a) ST-700-05; (b) ST-700-30; (c) ST-700-60; (d) IPF color code.**

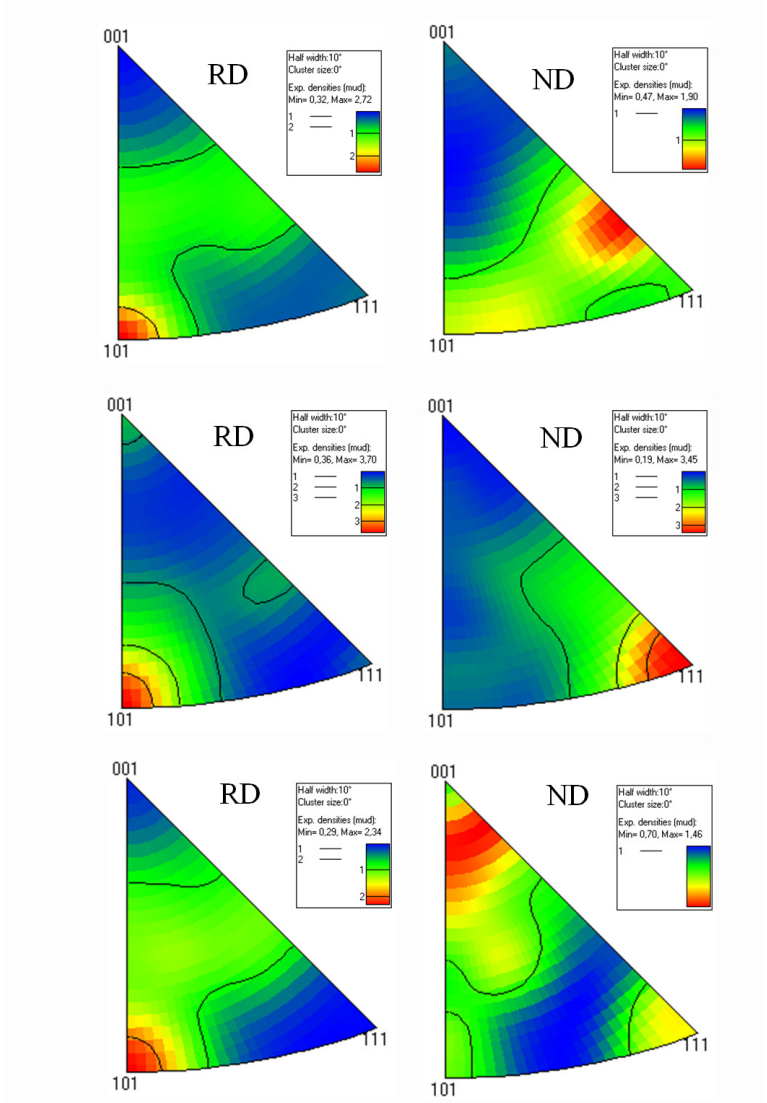

**Fig. 4. Inverse pole figures of Ti-20Zr-3Mo-3Sn alloy heated treated at: (a) ST-700-05; (b) ST-700-30; (c) ST-700-60. RD is parallel to tensile axis.**

## 4. Discussion

The superelasticity is due to the volume change of the lattice cell when the cubic crystal of b phase transforms into an orthorhombic crystal of a" martensite. This martensitic transformation follows an orientation relationships described as: $\{110\}_\beta \| (001)_{\alpha''}$ and $<111>_\beta \| [110]_{\alpha''}$ [2]. Thus, the transformation strain from parent β phase to SIM α" phase can be calculated for any direction of the lattice as a function of lattice parameters of both phases. The results show that the maximum of lattice strain, and thus the maximum of superelasticity, is obtained when the b phase is strained along a $<110>_\beta$ direction [2]. In the present study, the textures are different depending on the heat treatment duration. However, only the normal direction changes and the rolling direction keeps almost constant along the optimal $<110>_\beta$ direction (Fig. 4). That it why the three tested materials have the same maximum recoverable strain (Fig. 2d) as the main crystallographic direction along the tensile direction remains the same for the three samples. It has also to be noticed that these three types of $\{hkl\}_\beta<110>_\beta$ texture were already observed in other b titanium alloys [15-17].

Regarding the evolution of recoverable strain (Fig. 2d), it can be noticed that the superelasticity of the ST-700-30 specimen decreases significantly after the maximum value was reached, while it keeps more constant for the two other conditions. The unique difference lies in the texture, as all other microstructural parameters, including grain size (Fig. 3), are quite similar. By comparing the ST-700-05 and ST-700-30 conditions, which both reach the same maximum recoverable strain, one can conclude that a slightly less pronounced texture is beneficial to maintain the maximum value along a wider range of applied strain (ST-700-05) than a stronger texture for which the recoverable decreases immediately after the maximum is reached (ST-700-30). Indeed, a larger proportion of grains has a $<110>_\beta$ direction parallel to RD in the ST-700-30 specimen (Fig. 4b) than in the ST-700-05 specimen in which some grains have more random directions along RD (Fig. 4a). This feature probably gives a better ability to accommodate the applied strain when various crystallographic orientations are present in the microstructure. However, the main texture has to be kept with the $<110>_\beta$ direction along the rolling direction in order to obtain the maximum recoverable strain. Finally, with a heat treatment temperature chosen just above the b transus temperature, the shortest heat treatment time gives the highest and the most stable recoverable strain.

## 5. Conclusions

As a summary, the influence of thermal treatment duration on recovery strain of a novel superelastic Ti-20Zr-3Mo-3Sn (at.%) alloy for biomedical applications was investigated in this work. The results revealed that ST-700-05, ST-700-30 and ST-700-60 three samples have the same $\{hkl\}_\beta<110>_\beta$ type of texture, i.e. the crystallographic direction along the rolling direction remains constant but the normal direction changes depending on the heat treatment time.. The three conditions give a maximum recovery strain higher than 3.0%. Therefore, the Ti-20Zr-3Mo-3Sn alloy is not really sensitive to thermal treatment duration at the same temperature. Nevertheless, the shortest heat treatment time (ST-700-05) allows to stabilize the maximum value of recoverable strain during a wider range of applied strain due to a slightly less pronounced texture.

## Acknowledgments

J.J. Gao acknowledges the China Scholarship Council (CSC) for his Ph.D financial support (No. 2016-6329). The authors also acknowledge the CMEBA platform of the University of Rennes for providing access to SEM-EBSD facilities.

## References

[1] D.J. Wever, A.G. Veldhuizen, M.M. Sanders, J.M. Schakenraad, J.R. Van Horn, Biomater. 18 (1997) 1115–1120.

[2] H.Y. Kim, Y. Ikehara, J.I. Kim, H. Hosoda, S. Miyazaki, Acta Mater. 54 (2006) 2419–2429.

[3] T. Inamura, Y. Fukui, H. Hosoda, K. Wakashima, S. Miyazaki, Mater. Trans. 45 (2004) 1083–1089.

[4] F. Sun, Y.L. Hao, S. Nowak, T. Gloriant, P. Laheurte, F. Prima, J. Mech. Behav. Biomed. 4 (2011) 1864–1872.

[5] J.I. Kim, H.Y. Kim, T. Inamura, H. Hosoda, S. Miyazaki, Mater. Sci. Eng. A. 403 (2005) 334–339.

[6] H.Y. Kim, T. Sasaki, K. Okutsu, J.I. Kim, T. Inamura, H. Hosoda, S. Miyazaki, Acta Mater. 54 (2006) 423–433.

[7] A. Ramarolahy, P. Castany, F. Prima, P. Laheurte, I. Péron, T. Gloriant, J. Mech. Behav. Biomed. 9 (2012) 83–90.

[8] Y.L. Hao, Z.B. Zhang, S.J. Li, R. Yang, Acta Mater. 60 (2012) 2169–2177.

[9] M. Tahara, H.Y. Kim, H. Hosoda, T. Nam, S. Miyazaki, Mater. Sci. Eng. A. 527 (2010) 6844–6852.

[10] M. Besse, P. Castany, T. Gloriant, Acta Mater. 59 (2011) 5982–5988.

[11] M.F. Ijaz, D. Laillé, L. Héraud, D.-M. Gordin, P. Castany, T. Gloriant, Mater. Lett. 177 (2016) 39–41.

[12] M.F. Ijaz, H.Y. Kim, H. Hosoda, S. Miyazaki, Mater. Sci. Eng. C. 48 (2015) 11–20.

[13] L.L. Pavón, H.Y. Kim, H. Hosoda, S. Miyazaki, Scripta Mater. 95 (2015) 46–49.

[14] D.-M. Gordin, E. Delvat, R. Chelariu, G. Ungureanu, M. Besse, D. Laillé, T. Gloriant, Adv. Eng Mater. 10 (2008) 714–719.

[15] B. Sander, D. Raabe, Mater. Sci. Eng. A 479 (2008) 236-247.

[16] E. Bertrand, P. Castany, T. Gloriant, Acta Mater. 61 (2013) 511-518.

[17] Y. Yang, P. Castany, M. Cornen, I. Thibon, F. Prima, T. Gloriant, J. Alloys Compd. 591 (2014) 85-90.